J. Physiol. (1982), **323**, *pp.* 117–144
With 11 *text-figures*
Printed in Great Britain

INTRACELLULAR RECORDING FROM VERTEBRATE MYELINATED AXONS: MECHANISM OF THE DEPOLARIZING AFTERPOTENTIAL

BY ELLEN F. BARRETT AND JOHN N. BARRETT
From the Department of Physiology and Biophysics, University of Miami, P.O. Box 016430, Miami, FL 33101, U.S.A.

(*Received 2 April 1981*)

SUMMARY

1. Electrophysiological techniques are described which allow intracellular recording from peripheral myelinated axons of lizards and frogs for up to several hours. The sciatic and intramuscular axons studied here have resting potentials of −60 to −80 mV and action potentials (evoked by stimulation of the proximal nerve trunk) of 50–90 mV. They show a prominent depolarizing afterpotential (d.a.p.), which is present both in isolated axons and in axons still attached to their peripheral terminals. This d.a.p. has a peak amplitude of 5–20 mV at the resting potential, and decays with a half-time of 20–100 msec.

2. The peak amplitude of the d.a.p. is voltage-sensitive, increasing to up to 26 mV with membrane hyperpolarization. The d.a.p. disappears as the axon is depolarized to −60 to −45 mV, and does not appear to reverse with further depolarization.

3. The d.a.p. is not reduced when bath Ca is replaced by 2–10 mM divalent Mn or Ni. The d.a.p. is not reversed when axons depleted of Cl (by prolonged exposure to Cl-deficient, SO_4-enriched solutions) are bathed in Cl-rich solutions. These results suggest that the d.a.p. is not mediated by a conductance change specific for Ca or Cl ions. Partial substitution of tetramethylammonium for bath Na, or addition of 10^{-5} M-tetrodotoxin to the normal bathing solution, reduces the amplitude of both the action potential and the d.a.p.

4. The amplitude of the d.a.p. is not sensitive to bath [K] over the range 1–7·5 mM, provided that all measurements are made at the same holding potential. This result argues that the d.a.p. is not mediated by accumulation of K outside the active axon.

5. Treatments expected to inhibit the Na–K exchange pump (cooling from 25 to 10 °C, or 0·15 mM-ouabain) do not enlarge or prolong the d.a.p., although they do abolish a slower hyperpolarizing afterpotential seen following repetitive stimulation.

6. The passive voltage response of the axon to small injected pulses of depolarizing or hyperpolarizing current shows a prominent, slowly decaying component with a time course similar to that of the d.a.p. Depolarizing current reduces the input resistance of the axon, and increases the rate of decay of both the passive voltage response and the d.a.p. There is a slight conductance increase during the peak of the d.a.p., but the same conductance increase can be produced by a comparable passive depolarization.

7. We conclude that the d.a.p. is due mainly to a passive capacitative current, probably resulting from discharge of the internodal axonal membrane capacitance through a resistive current pathway beneath or through the myelin sheath. We suggest that this slow capacitative discharge becomes evident as soon as most of the nodal ionic channels activated during the action potential have closed. An electrical model of the myelinated axon that incorporates the postulated internodal leakage pathway can account both for the prolonged d.a.p. recorded inside the axon, and for the potential profile recorded extra-axonally in or near the internodal periaxonal space.

INTRODUCTION

Previous studies have shown that action potential propagation in myelinated axons is saltatory, i.e. that the major ionic and capacitative currents associated with the action potential flow mainly from node to node, since the multilamellar myelin sheath inhibits current flow across internodal membranes (reviewed in Stämpfli, 1952; Tasaki, 1953; Hodgkin, 1964). Because the voltage-sensitive conductances in the node have relatively fast kinetics, and because the input resistance and capacitance of nodal membranes and the capacitance of the myelin sheath are relatively low, this 'node-to-node' model for the electrical behaviour of myelinated axons predicts that the passive electrical response of the axon should be relatively fast, and that the ionic and capacitative currents associated with the action potential should cease flowing within a few milliseconds. However, we present potentials recorded intracellularly from myelinated peripheral axons of lizards and frogs which show a prominent, slowly decaying component with a time course of several hundred milliseconds. This slowly decaying component is evident in the passive electrical response of the axon to applied hyperpolarizing current pulses, and as a depolarizing afterpotential (d.a.p.) following the action potential. Further experiments described here indicate that the d.a.p. is not due to any known ionic conductance system, or to extracellular accumulation of K. Taken together, these findings support the hypothesis that the slowly decaying voltage response reflects a passive electrical property of the intact myelinated axon. If this hypothesis proves true, then the classical electrical model of the resting myelinated axon must be modified to account for the slowly decaying component of the voltage transient. We present a revised model in which the large capacitance of the internodal axon membrane discharges via an internodal leakage pathway. Preliminary calculations suggest that the most likely routes for the postulated internodal leakage current are under the myelin sheath, through the periaxonal space and the innermost layer of Schwann cell cytoplasm (see Mugnaini, Osen, Schnapp & Friedrich, 1977).

We suspect that the d.a.p. we record accounts for much of the prolonged superexcitable period that follows the action potential in frog axons (Raymond, 1979).

METHODS

Preparation and solutions

Most intracellular recordings were made in the large myelinated motor axons (total fibre diameter up to 10 μm, axon diameter up to 7 μm) that innervate the thin (one to two muscle cell layers) dewlap extensor muscle in the jaw of small lizards (*Anolis sagrei*) common in Florida. Some experiments used motor axons in the thin cutaneous pectoris muscle of small frogs (*Rana pipiens*). A few experiments used axons in the isolated frog sciatic nerve, or axons in the *in situ* rat ventral root. The neuromuscular preparations were pinned flat against a glass coverslip and viewed at 700 × magnification with Nomarski differential interference contrast optics. Frog sciatic nerve trunks were placed on a glass coverslip coated with a layer of collagen and polylysine (to enhance axon–substrate adhesion) and teased apart into small axon bundles, which were also viewed at high magnification. The layer of bathing solution that covered these preparations was kept thin to improve visibility.

Preparations were perfused with standard salt solutions (mM: 157 NaCl, 4 KCl, 2 $CaCl_2$ for lizard; 115 NaCl, 2 KCl, 1·8 $CaCl_2$ for frog), all of which contained in addition 5 mM-glucose and 1 mM-PIPES buffer. Modifications of these standard solutions are described where appropriate in the text. Bath pH was maintained in the range 7·2–7·5, monitored colorimetrically using small amounts of the indicator dye, Phenol Red (1 mg/l.). The bathing solution could be changed within a few minutes using a perfusion pump with equalized inflow and outflow. Most experiments were performed at room temperature (20–25 °C).

The nerve trunk was stimulated with brief (0·1 msec) pulses administered via a suction electrode. In neuromuscular preparations muscle contractions were inhibited by blocking transmission pre- or post-synaptically (presynaptic blockers: 0·5–10 mM-Mn, Mg, Ni or Co, with or without lowered bath [Ca]; post-synaptic blockers: 10^{-4}–10^{-6} M-curare or chronic exposure to carbachol). These blocking agents did not produce the depolarizing afterpotential (d.a.p.) studied here because d.a.p.s similar to those recorded in the axons of muscle nerves were recorded from axons in the isolated sciatic nerve in the absence of neuromuscular blocking agents, and d.a.p.s recorded in the presence and absence of Mn (curare present throughout) were similar (Fig. 4). Axons coursing across a muscle were assumed to be motor. Many of these axons could be visually traced to a motor nerve terminal. In a few cases curare was withdrawn at the end of a recording session, and an action potential was evoked by passing dépolarizing current into the axon through the intracellular electrode. In all cases so tested, several muscle fibres contracted, further verifying that the electrode had been in a motor axon.

Micro-electrode construction and placement

Short-shafted glass micropipettes were pulled with a Brown-Flaming micropipette puller (Sutter Instrument Co.). The micropipettes were filled with 0·2 M-K_2SO_4, and had resistances of 50–200 MΩ. More concentrated filling solutions (1M-KCl or 0·5 M-K_2SO_4) were used occasionally, but impaled axons remained electrically stable for longer periods of time with the less concentrated filling solutions. Current was passed through the recording electrode using a standard Wheatstone bridge arrangement. Electrodes used to pass current were first bevelled (method of Ogden, Citron & Pierantoni, 1978) to reduce their resistance.

The micro-electrode was centred over the internode of a visualized surface axon using a mechanical micromanipulator (built by C. Freites), and lowered until it visually depressed the surface of the myelin sheath. The micro-electrode was then 'tapped' into the axon by applying brief pulses (10–100 V, 1 msec) across the plates of a home-made piezoelectric device attached to the micro-electrode shaft. Activation of this device produced a rapid forward movement of the electrode tip.

Impalements were most stable when the horizontal projecton of the micro-electrode shaft was parallel to the long axis of the axon (see also Fuchs & Getting, 1980). Most impalements were made in the internodal region; potentials recorded here were indistinguishable from those recorded within a few microns of a visualized node of Ranvier, as expected from the long space constant of myelinated axons (see Discussion).

Successful axonal impalements were signalled by a sudden drop in potential (−50 to −80 mV in standard salt solutions). Axons with initial resting potentials of −50 mV often hyperpolarized over time to reach a stable level of −60 to −80 mV. Our best resting potentials (−70 to −80 mV)

compare favourably with the average value of −71 mV estimated for unimpaled frog axons using a bridge balancing technique (Huxley & Stämpfli, 1951). Since the focus of this study is a slow afterpotential, we adjusted the capacitance compensation setting of the input preamplifier (Picometric 181) to reduce electrical noise, while still holding the time constant of the recording system to less than 0·1 msec. This procedure selectively attenuates the amplitude of high-frequency signals like the action potential, but does not alter the amplitude or time course of a slow potential like the d.a.p. Thus in the records presented here, peak action potential amplitudes (in response to stimulation of the proximal nerve trunk) are only 50–80 mV and show little or no overshoot, considerably less than the average amplitude of 102–116 mV estimated by Huxley & Stämpfli (1951) and Tasaki & Frank (1955), or the largest peak amplitudes (> 110 mV) reported in the early intracellular studies of Woodbury (1952) and Hardy (1973). Action potential amplitudes increase as capacitance compensation is increased. In recent studies using what we believe to be optimal compensation settings, action potential amplitudes of 100 mV have been obtained (K. Scappaticci, unpublished observations). Also, our experiments were generally done at somewhat higher temperatures (20–25 °C) than those used in earlier work (~ 17 °C), and in our hands low temperatures tended to increase action potential amplitudes (Fig. 6).

Some impaled axons remained electrically stable for more than 60 min, and could be maintained through several careful solution changes. The microscope light source was switched off during the recordings to avoid overheating the axon.

In a few cases after 'tapping' the micro-electrode into the myelin sheath we recorded action potentials with little or no preceding resting potential (Fig. 9*C*). These action potentials were followed by a prolonged hyperpolarizing afterpotential, instead of the depolarizing afterpotential recorded when the resting potential was more hyperpolarized than −50 mV. Since the depolarizing afterpotential in a given axon was never reversed by depolarizing current (see Results) we suspect that the few recordings showing hyperpolarizing afterpotentials resulted from electrode placement within the myelin sheath or periaxonal space (see Fig. 9, Discussion).

RESULTS

Depolarizing afterpotential: origin and voltage sensitivity

Fig. 1 shows action potentials and afterpotentials recorded intracellularly from lizard motor (*A*) and frog motor and sciatic (*B* and *C*) axons following stimulation of the proximal nerve trunk. These axons, and all axons with resting potentials of 60 mV or better, show a prominent, prolonged depolarizing afterpotential (d.a.p.). In a sample of eighteen intramuscular lizard axons with a resting potential of −60 mV or better, the peak amplitude of the d.a.p. ranged from 5 to 20 mV (mean 10·6 ± 3·3 mV S.D.). The d.a.p. usually decayed monotonically, sometimes exponentially. The half-time of decay in this eighteen-axon sample ranged from 20 to 98 msec (mean 55·5 msec ± 19·4 msec S.D.). The amplitude and time course of the d.a.p.s measured in frog intramuscular axons also fell within these ranges. Occasionally the d.a.p. began with a brief plateau (Fig. 6*A*) or was preceded by a brief hyperpolarizing 'dip'. This dip, whose amplitude was enhanced by depolarization, is probably due to the nodal K conductance.

The fact that a d.a.p. is recorded in sciatic nerve axons lacking central and peripheral terminals (Fig. 1*C*) indicates that this potential originates in the myelinated axon itself.

The amplitude of the d.a.p. is sensitive to membrane potential in the region around the resting potential. Fig. 2*A* shows action potential–d.a.p. sequences evoked in a lizard axon at various imposed levels of membrane potential, and the triangles in Fig. 2*C* plot peak d.a.p. amplitude as a function of membrane potential in this axon. D.a.p. amplitude increased with hyperpolarization. In the axon of Fig. 2 peak d.a.p.

amplitude increased from 10 mV at the resting potential (−70 mV) to 18 mV when the axon was hyperpolarized to −80 mV. In another lizard axon peak d.a.p. amplitude increased from 16 mV at −75 mV to 26 mV at −95 mV. In both axons d.a.p. amplitude decreased approximately linearly with depolarization. The d.a.p. showed no reversal potential. It disappeared at depolarized membrane potentials (extrapolated values −58 mV and −46 mV in the two axons tested in detail). The

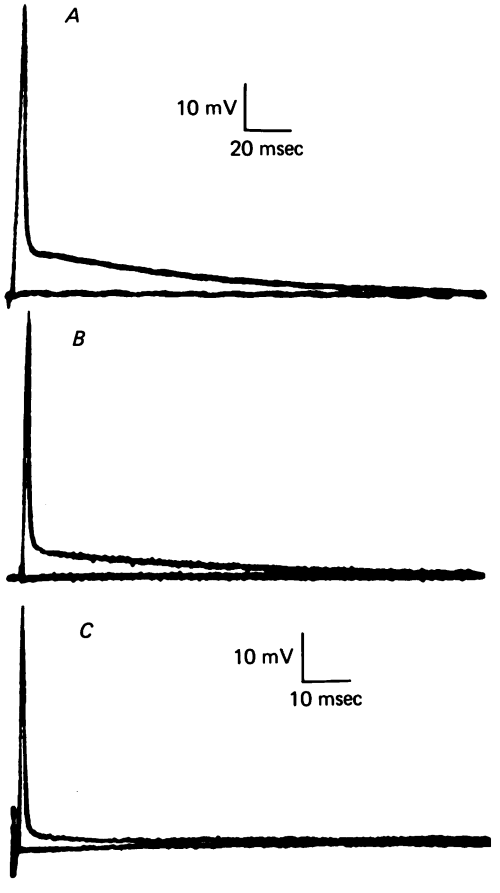

Fig. 1. Action potentials and depolarizing afterpotentials recorded intracellularly from lizard (*A*) and frog (*B* and *C*) myelinated peripheral axons following suprathreshold stimulation of the proximal nerve trunk. These records (and those in Figs. 3, 4, 6 and 9*C*) also include a voltage trace following subthreshold nerve trunk stimulation to show the stimulus artifact and base line. Same calibrations in *A* and *B*. *A*, lizard dewlap extensor muscle, 2 mM-Mn, 1 mM-Ca. *B*, frog cutaneous pectoris muscle, 6 mM-Ca, 2 mM-Mg, 10^{-5} M-curare. *C*, frog sciatic nerve, 2 mM-Ca, 2 mM-Mg.

d.a.p. disappeared before depolarization blockade of action potential invasion. Similar voltage-dependent variations in d.a.p. amplitude were observed in all of more than twenty lizard and frog axons tested.

The voltage sensitivity of d.a.p. amplitude was not merely an artifact of passing current through the recording electrode, because d.a.p. amplitude varied in a similar manner in axons which depolarized or hyperpolarized spontaneously, or in response

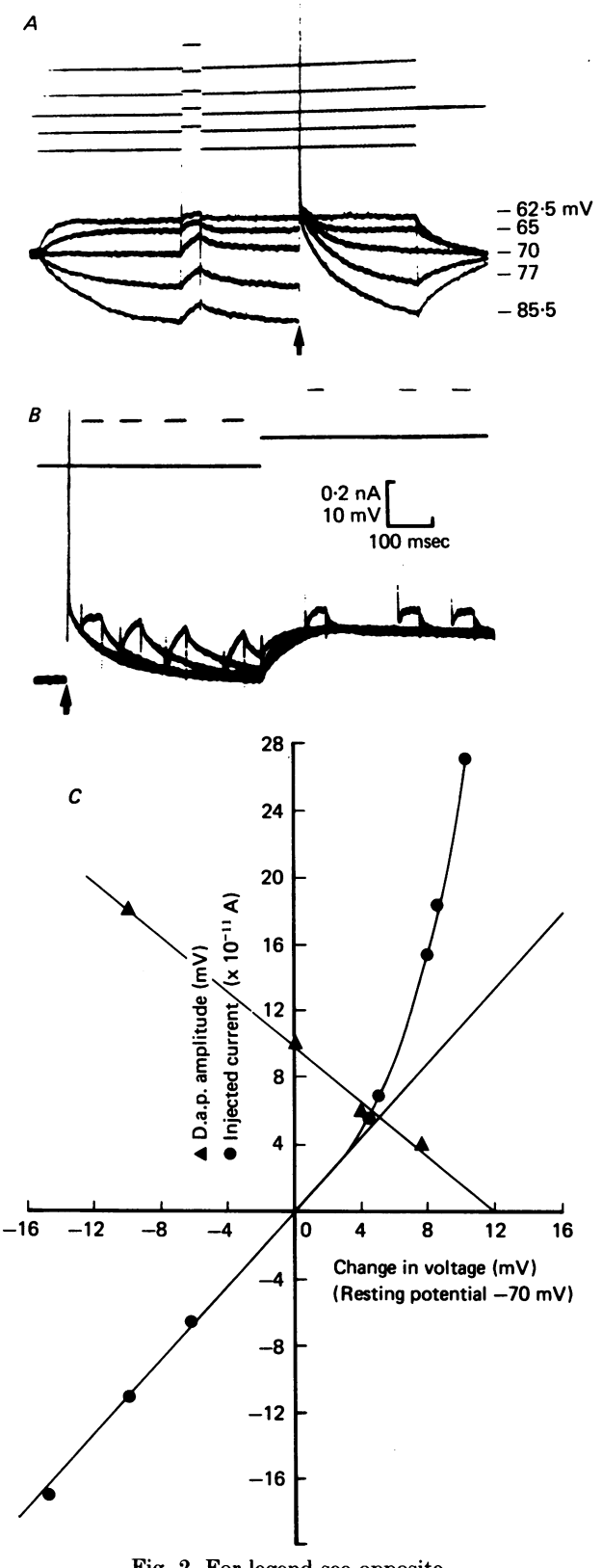

Fig. 2. For legend see opposite.

to changes in bath [K]. For example, when an axon was first penetrated, the resting potential was frequently only −50 mV, and little or no d.a.p. was observed. In many cases the axon then spontaneously hyperpolarized to a steady level of −60 to −70 mV (presumably as the axonal membrane 'sealed' around the electrode), and as it did so the d.a.p. appeared and grew in amplitude.

The half-decay time of the d.a.p. also varied with membrane potential, decreasing with depolarization and increasing to 90–110 msec in axons hyperpolarized to −90 to −100 mV. In axons at the resting potential the d.a.p. usually decayed more rapidly at early times; the late time course of the d.a.p. was often similar to that recorded at more hyperpolarized potentials.

Most of the experiments described henceforth were designed to test three possible mechanisms for this d.a.p.: (1) a passive capacitative discharge of internodal axon membranes, (2) an ionic conductance change or (3) an accumulation of K outside the active axon.

Passive electrotonic response: similarity to the depolarizing afterpotential

Fig. 3 shows the passive response of a lizard axon to injection of hyperpolarizing current pulses of varying duration, along with an action potential–d.a.p. sequence evoked in that axon by stimulation of the proximal nerve trunk. The passive electrotonic response has both fast and slow components, that are evident both during and after the current pulse. In this and two other well characterized axons the slowly decaying passive component, most prominent following long current pulses, has a time course similar to that of the d.a.p. The electrotonic response to small, subthreshold depolarizing current pulses also has a prominent slow component (Fig. 2*A*). The fact that a slowly decaying voltage response of the same polarity as the stimulus can be seen following both hyperpolarizing and sub- and suprathreshold depolarizing current pulses suggests that this slow component reflects a passive membrane property of the axon. Thus it appears that intact myelinated axons have a significant passive transmembrane current pathway with a much longer passive time constant (about 100 msec) than has hitherto been suspected, and that most or

Fig. 2. Voltage-dependent conductance changes and voltage dependence of the depolarizing afterpotential in a lizard motor axon bathed in 1 mM-Ca, 0·5 mM-Mn. Resting potential −70 mV. In *A* and *B* lower traces show recorded voltage, upper traces indicate current applied through the recording electrode, and arrows indicate suprathreshold stimulation of the proximal nerve trunk. Same calibrations in *A* and *B*. *A*, in each of the five superimposed voltage traces the membrane potential of the axon was changed to the indicated level by applying a current step. Then a brief (50 msec) depolarizing current pulse was applied, and an action potential (top truncated) and d.a.p. were evoked. Depolarization increases axonal input conductance and reduces the peak amplitude of the d.a.p. *B*, in each of the seven superimposed voltage traces a subthreshold 50 msec depolarizing current pulse was applied at various times during either the d.a.p. or a subsequent 400 msec applied depolarization. Axonal input conductance is increased at the beginning of the d.a.p., and during a passive depolarization to the level of the peak of the d.a.p. *C*, circles plot the steady-state current–voltage relationship and triangles plot d.a.p. amplitude as a function of membrane voltage measured from records like those in *A*. The resting input resistance of this axon (measured from the slope of the line through the resting potential (origin) and points hyperpolarized to the resting potential) was 86 MΩ.

all of the d.a.p. is a passive capacitative discharge of an internodal membrane capacitance charged during the action potential. Possible internodal pathways for this slow discharge are considered in the Discussion.

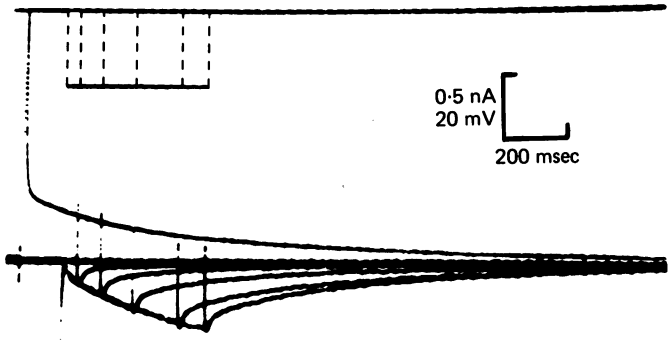

Fig. 3. Similar time courses of the depolarizing afterpotential and the slowly decaying component of the passive electrotonic response of a lizard motor axon in 2 mM-Ni. The lower trace superimposes an action potential–d.a.p. sequence (evoked by stimulating the proximal nerve trunk) and the passive voltage response of this axon to applied hyperpolarizing current pulses of varying duration. Upper trace shows current pulses applied through the recording electrode (onset and offsets retouched for clarity).

Conductance increase in depolarized axons

Fig. 2*A* shows the membrane potential changes produced by injecting long (> 200 msec) current pulses into a lizard axon. The response to subthreshold depolarizing current pulses has a smaller amplitude and a faster rise time than the response to comparable hyperpolarizing current pulses, indicating that depolarization decreases the input resistance and time constant of the axon. Circles in Fig. 2*C* plot the steady-state current–voltage relationship measured from these data. The depolarization-induced decrease in input resistance seen in this and five other tested axons is most likely due to activation of the nodal K conductance. The resting input resistance of this axon (measured in the hyperpolarized region of the curve) is 86 MΩ. Resting input resistances ranged from 67 to 118 MΩ (mean 88 MΩ) in eight lizard motor axons. These measurements of axonal input resistance are somewhat higher than those that would be expected from Tasaki's (1953, 1955) and Conti, Hille, Neumcke, Nonner & Stämpfli's (1976) measurements of the membrane resistance of single frog and toad sciatic nodes (40–80 MΩ by Tasaki; 46–124 MΩ by Conti *et al.*). One likely reason for this discrepancy is that Tasaki's measurement technique depolarized the nodes; in our hands depolarization reduced axonal input resistance to 30 MΩ or less. Other reasons for our large measured input resistance values are the smaller size of our intramuscular axons (8–10 μm fibre diameter compared to 12–14 μm in Tasaki's and 14–18 μm in Conti *et al.*'s sciatic axons), and the fact that many of our axons were impaled electrically close to their peripheral terminals. Our largest input resistance values come from axons whose motor terminals were visible in the microscope field (< 100 μm from the site of impalement).

Measurements of the voltage–time integral (area) of the response to brief, subthreshold current pulses (see Barrett & Barrett, 1976) indicate that axonal input

conductance is increased during the peak of the d.a.p. (Fig. 2*B*). However, the conductance increase during the d.a.p. is no greater than that achieved by injecting current sufficient to depolarize the axon to the potential at the peak of the d.a.p. (Fig. 2*B*). Thus an increase in membrane conductance of the magnitude seen during the d.a.p. does not require a prior action potential, and may in fact be a consequence, rather than a cause, of the d.a.p.

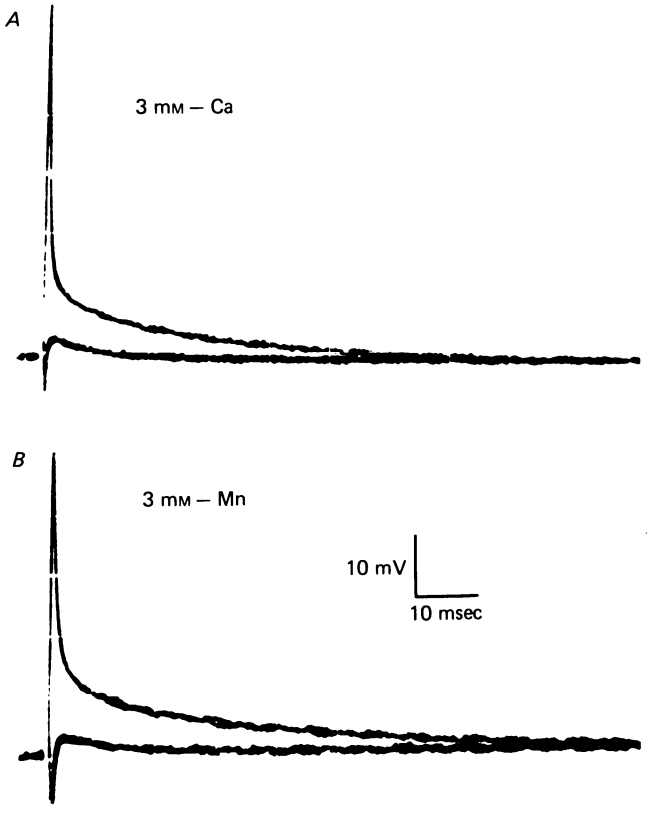

Fig. 4. Action potentials and depolarizing afterpotentials evoked in a lizard motor axon bathed in 3 mM-Ca (*A*) or 3 mM-Mn (*B*). 10^{-5} M-curare present throughout. Mn reduces the amplitude of the action potential, and slightly increases and prolongs the d.a.p.

Ionic dependence of the depolarizing afterpotential

Calcium. To test whether a slow Ca influx might contribute to the d.a.p., we varied bath [Ca] or added Mn or Ni, divalent cations which block Ca currents in many preparations. The records of Figs. 2 and 3, obtained in 0·5 mM-Mn and 2 mM-Ni, respectively, show that Mn and Ni do not block the d.a.p. Reducing bath [Ca] without adding other divalent cations reduces the amplitude of the d.a.p. at the resting potential. However, even in 0·1 mM-Ca the amplitude of the d.a.p. can still be increased by passing hyperpolarizing current into the axon. Increasing bath [Ca] above the normal 2 mM increases d.a.p. amplitude, but these effects of [Ca] on d.a.p. amplitude are not specific for Ca, since Mn and Ni have similar effects. For example, Fig. 4 shows records obtained in one axon bathed in 3 mM-Ca (*A*) and then in 3 mM-Mn

(*B*, no added Ca). The d.a.p.s recorded in Ca and Mn are remarkably similar. Mn reduces the amplitude of the action potential, consistent with its inhibitory effect on the Na current in frog nodes (Århem, 1980). These results suggest that Ca influx does not contribute importantly to the d.a.p. The effect of divalent cation concentration on d.a.p. amplitude is probably due to these cations' effect on membrane surface potential. High divalent cation concentrations reduce the negative surface charge on the external axon membrane, thus hyperpolarizing the effective transmembrane electric field, which increases d.a.p. amplitude (Fig. 2*A* and *C*). Conversely, low divalent cation concentrations depolarize the effective transmembrane field, which decreases d.a.p. amplitude (see Hille, Woodhull & Shapiro, 1975, for a discussion of surface charge effects on Na current).

Chloride. To determine whether the d.a.p. might be mediated by Cl efflux, we attempted to reverse any transmembrane electrochemical gradient for Cl by depleting the axon of Cl (via a half-hour exposure to an isosmotic, Cl-free, SO_4-substituted bathing solution), and then exposing these Cl-depleted axons to a normal, Cl-containing solution. This procedure should favour Cl influx, and would thus reverse any Cl-dependent afterpotential. Since no d.a.p. reversal was observed, we conclude that a Cl current is not the major mechanism of the d.a.p. Variations in bath [HCO_3] likewise had little effect on the d.a.p.

Sodium. Reductions in bath [Na] ($\frac{1}{2}$–$\frac{2}{3}$ of bath Na replaced by tetramethylammonium) reduced the amplitudes of both the action potential and the d.a.p. Both potentials were also reduced, and subsequently abolished, by addition of 10^{-5}–10^{-6} M-tetrodotoxin (TTX) to the normal bath solution. Neither treatment produced any consistent change in the resting potential. In TTX the amplitude reductions of both the action potential and the d.a.p. often occurred in a sudden, stepwise manner, perhaps signalling conduction failure at a nearby node. Because TTX and reductions in [Na] alter the action potential as well as the d.a.p., these experiments give no conclusive evidence concerning a possible Na contribution to the d.a.p.

Potassium. Depolarizing afterpotentials recorded or inferred in a variety of neurone somata and axons are often attributed to an accumulation of K in a restricted extracellular space surrounding the active neurone (reviewed in Zucker, 1974). Accordingly, we tested whether the d.a.p. in peripheral myelinated axons might be due to extracellular K accumulation, either in a space accessible to the bath (e.g. around the node), or in a relatively inaccessible periaxonal space (e.g. under the myelin sheath in the internodal region).

If the d.a.p. were due to accumulation of K in an accessible space, its amplitude should vary with bath [K]. Specifically, for a given rate of K efflux from the active axon, d.a.p. amplitude should increase as bath [K] is reduced, and decrease as bath [K] is increased. This is because the K leaving the active axon changes the transmembrane K equilibrium potential (E_K) more when bath [K] is low than when bath [K] is high. The curves in Fig. 5 plot this expected dependence of the change in E_K on bath [K], calculated using the Nernst equation. As indicated, the curves were calculated assuming that K efflux from the active axon temporarily increases extracellular [K] by 1, 2 or 4 mM. The exact relationship between the change in E_K and the change in the amplitude of a K-dependent depolarizing afterpotential will depend on the permeability characteristics of the axonal membrane, but in all cases

d.a.p. amplitude would be expected to decrease as bath [K] increases, by an amount proportional to the change in E_K.

We tested this prediction by measuring peak d.a.p. amplitude in five axons as bath [K] was varied over the range 1–7·5 mM (higher [K] often blocked action potential propagation). Because d.a.p. amplitude is so sensitive to membrane potential (Fig. 2), all amplitude measurements were made at a membrane potential of −70 mV, maintained by passing small steady currents through the recording electrode. The circles in Fig. 5 show the averaged results of these d.a.p. amplitude measurements

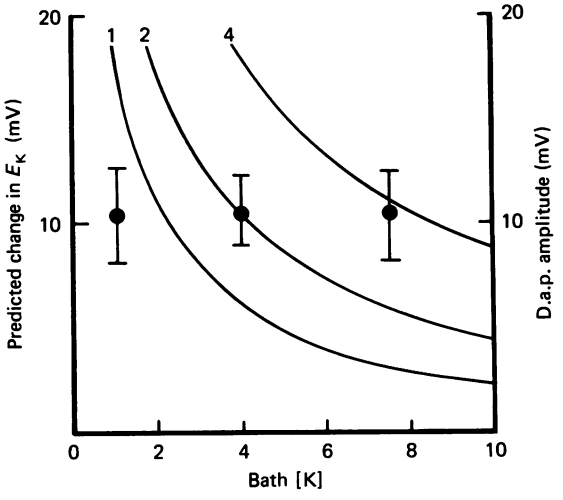

Fig. 5. Effects of bath [K] on the depolarizing afterpotential. Circles indicate the mean, and bars the range, of the peak amplitude of the d.a.p. (right ordinate) in at least five lizard motor axons bathed in 1, 4 and 7·5 mM-K. D.a.p. amplitudes were measured from the same baseline membrane potential (−70 mV), maintained by passing current through the recording electrode. The curves labelled 1, 2 and 4 show calculated changes in the transmembrane K equilibrium potential (E_K, left ordinate) if the K efflux following a single action potential increases extracellular [K] by 1, 2 or 4 mM, respectively. Recorded d.a.p. amplitudes show no tendency to change with bath [K], suggesting that the d.a.p. is not due to K accumulation around the active axon.

in 1, 4 and 7·5 mM-K. These data indicate that when membrane potential is held constant, d.a.p. amplitude does not vary with bath [K], suggesting that the d.a.p. in myelinated axons is not due to a build-up of K around the node. When no steady currents were injected, the resting membrane potential varied with bath [K], hyperpolarizing slightly in 1 mM-K and depolarizing slightly (by 3–10 mV) in 7·5 mM-K. These membrane potential changes had the same effect on d.a.p. amplitude as similar membrane potential changes occurring at constant bath [K].

Temperature dependence of axonal afterpotentials

We also considered the possibility that the d.a.p. might result from an accumulation of K in a restricted extracellular space that is completely or relatively inaccessible to the bath (e.g. the periaxonal space in the internodal region). Since any K added to this space during axonal activity could not readily leave by diffusion, the rate of decay of [K] in this space would be expected to be determined by the rate of active

K uptake into the axon or Schwann cell. If so, the rate of decay of any K-dependent d.a.p. should be sensitive to treatments which inhibit the Na–K exchange pump, such as low temperature or ouabain. However, we found that 0·15 mM-ouabain (not shown) and temperature changes in the range 10–25 °C had little effect on the rate of decay of the d.a.p. studied here. For example, Fig. 6*A* and *B* shows d.a.p.s recorded in a frog motor axon at 25 and 15·5 °C. The action potential has a greater amplitude and duration at the lower temperature, but the d.a.p. is smaller than, and decays over

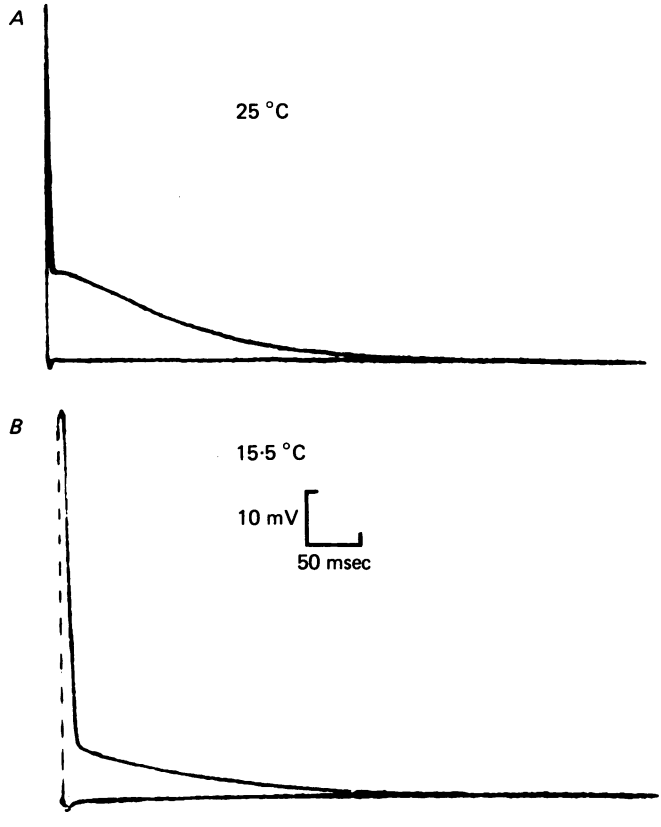

Fig. 6. Effect of temperature on the action potential and depolarizing afterpotential in a frog motor axon bathed in 2 mM-Ca, 1 mM-Mn and 10^{-5} M-curare. *A*, 25 °C *B*, 15·5 °C. Lowering the bath temperature increases the amplitude and duration of the action potential and reduces the amplitude and duration of the d.a.p. The action potential in *B* is truncated, and its rising phase is retouched for clarity.

about the same time course as, the d.a.p. measured at 25 °C. The smaller amplitude of the d.a.p. at lower temperatures may have been due in part to a slight (< 5 mV) axonal depolarization. Similar changes in the action potential and d.a.p. were seen in two additional temperature change cycles in this same axon and in two additional lizard and frog axons. In no case did lowering the bath temperature to 10–15 °C increase or prolong the d.a.p. recorded after a single action potential. Thus the amplitude and duration of this d.a.p. do not appear to be controlled by a temperature-sensitive active uptake of K.

Repetitive stimulation reveals the existence of slower afterpotentials which are

temperature- and ouabain-sensitive, and thus involve an electrogenic ion pump. Fig. 7 *A* and *B* shows afterpotentials recorded in a frog axon following a brief train of 50 Hz stimulation at 25 and 14 °C. (Note that the time scales in this Figure are much slower than in the other Figures.) The afterpotential recorded at the higher temperature has an initial depolarizing component (the d.a.p. of Figs. 1 and 6), which is followed by a slowly decaying hyperpolarization. This hyperpolarizing afterpotential is even more

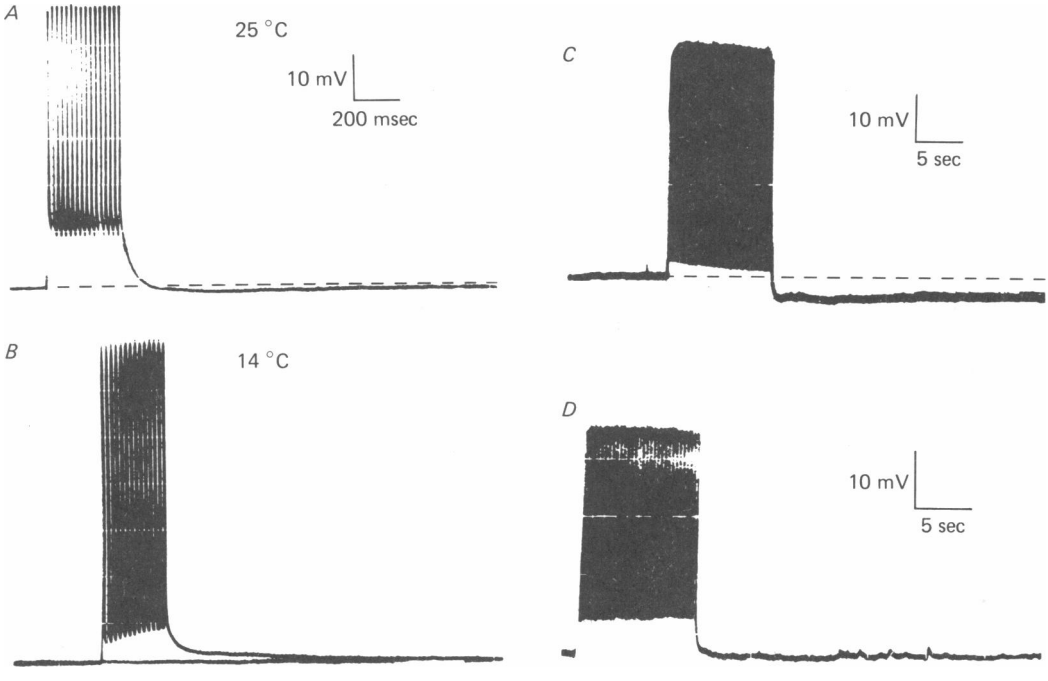

Fig. 7. Effect of temperature and ouabain on afterpotentials following repetitive activity in motor axons. *A* and *B*. Frog motor axon (same axon as Fig. 6). A train of 14–16 impulses at 50 Hz is followed by a prolonged hyperpolarizing afterpotential at 25 °C (*A*), and a prolonged depolarizing afterpotential at 14 °C (*B*). Same calibrations in *A* and *B*. *C* and *D*, lizard motor axon bathed in 2 mM-Ca and 10^{-5} M-curare. Stimulation at 15 Hz for 10 sec results in a prolonged hyperpolarizing afterpotential (*C*) that is absent in 0·15 mM-ouabain (*D*). Base lines added for clarity in *A* and *C*.

pronounced following longer, faster stimulus trains (Fig. 7 *C*). The slow hyperpolarization disappears at lower temperatures (Fig. 7 *B*) or in the presence of 0·15 mM-ouabain (Fig. 7 *D*), suggesting that it is due to an electrogenic Na–K exchange pump. At cold temperatures a train of action potentials is followed by a very slow depolarizing afterpotential (Fig. 7 *B*), whose magnitude increases with the frequency and duration of the preceding stimulus train. This very slow depolarizing afterpotential may reflect an accumulation and subsequent diffusion-limited decay of [K] in the space around the active axon.

In summary, the effects of bath [K], temperature and ouabain on the early (< 500 msec duration) d.a.p. suggest that this potential is *not* due to an accumulation of K in the periaxonal space. However, K movements probably do contribute to the slower hyperpolarizing and depolarizing afterpotentials seen following repetitive stimulation.

DISCUSSION

The experiments presented here use intracellular recording techniques to characterize a prominent depolarizing afterpotential (d.a.p.) in myelinated motor axons of frogs and lizards. Our results indicate that this slowly decaying d.a.p. is not due to a conductance change specific for Ca or Cl, or to K accumulation outside the active axon. Instead the d.a.p. appears to be primarily a passive capacitative discharge, because the voltage transient evoked by a hyperpolarizing current pulse has a slowly decaying component whose time course resembles that of the d.a.p. (Figs. 2 and 3). Thus it appears that frog and lizard myelinated axons have a slow (time constant 50–150 msec) current pathway, in addition to the fast (time constant $\sim$ 1 msec) pathway described in the classical literature.

The prolonged depolarizing afterpotential so prominent in our intracellular records has not, to our knowledge, been recorded in previous studies of frog axons. Most earlier studies concentrated on the fast voltage changes and currents associated with the action potential itself. Also, standard voltage-clamp techniques electrically isolate the internodal regions surrounding the clamped node with vaseline seals and exposure to a non-conducting medium (sucrose or air), thus reducing the internodal current that most likely produces the d.a.p. in intact, *in situ* axons. Some early intracellular recordings show what may be the beginning of a depolarizing afterpotential (e.g. Fig. 5 in Woodbury, 1952), but this was not a consistent finding, perhaps because the d.a.p. is absent when the axonal membrane is depolarized (Fig. 2).

We considered the possibility that the internodal leakage pathway postulated in our model for the d.a.p. (Fig. 8*C*) might be an artifact produced by micro-electrode penetration of the myelin sheath. That is, the electrode track might itself introduce a relatively low resistance leakage pathway from the internodal periaxonal space to the bath. However, at least two independent lines of evidence convince us that the d.a.p. is a real afterpotential that occurs in intact, non-impaled axons. First, a large d.a.p. persists even after blocking action potential generation in adjacent nodes by injecting hyperpolarizing current into the internodal recording site. If the d.a.p. were generated only by the impaled internode, then its amplitude should be proportional to the time integral of the action potential depolarization. The fact that injected hyperpolarizing current attenuates the recorded d.a.p. much less than the recorded action potential amplitude argues that a significant portion of the d.a.p. must originate in adjacent non-impaled internodes. Since the axonal space constant is longer for slow events such as the d.a.p. than for fast events such as the action potential (see below), it is not surprising that the d.a.p. decreases less than the action potential in response to local node block. Secondly, the intracellularly recorded d.a.p. bears many similarities to the negative afterpotential recorded extracellularly from frog sciatic A fibres: the magnitudes of the d.a.p. and the negative afterpotential are similarly affected by changes in bath [Ca] and [K] and cooling (compare Figs. 4 and 6 with the results of Gasser, 1937). Also, the time course of the intracellularly recorded d.a.p. is very similar to the time course of axonal superexcitability measured following action potentials in single, unimpaled frog sciatic axons (see Raymond, 1979, who also reviews earlier work on superexcitability). Both the d.a.p. and superexcitability are absent in depolarized axons, and both cumulate less than

linearly following short bursts of action potentials (compare the results in Figs. 2 and 7 with those of Raymond, 1979). Following intense activity, the depolarizing–hyperpolarizing afterpotential sequence we observe (Fig. 7*A* and *C*) is similar to the supernormal–subnormal excitability sequence observed by Raymond (1979, his Figs. 7 and 15; see also Gasser, 1937). Thus available evidence suggests that the d.a.p. we record intracellularly also occurs in non-impaled myelinated axons, and contributes importantly to the post-stimulus superexcitable period in these axons.

Passive capacitative current model for the depolarizing afterpotential

Analogue circuits of myelinated axon

Fig. 8 shows three electrical models of the myelinated axon, each superimposed on a crude diagram of a node–internode sequence. Part *A* shows the circuit suggested by most earlier studies, which lumps together the resistance and capacitance of the internodal axonal membrane and the membrane layers of the myelin sheath. With this model, current injected into a node can leave the axon either through a node (major pathway) or through the internode-myelin pathway (a minor pathway, since the resistance of the internodal axon and myelin membranes in series, R_{im}, is very large, while the capacitance of internodal and myelin membranes in series, C_{im}, is very small). In this classical model both the major and minor current pathways have short time constants, because both the nodal capacitance, C_N, and the lumped effective internodal capacitance, C_{im}, are relatively small (1–3 pF). To account for the long time constant component of the passive response of these axons (Fig. 3), we propose an additional internodal current pathway, shown in Fig. 8*B*, which permits the large capacitance of the internodal axonal membrane, C_i, to discharge to the bath via an internodal leakage resistance, R_{il}, under or through the myelin sheath.

Simulation of the depolarizing afterpotential

To estimate the magnitude of the postulated internodal leakage resistance, we first simplifed the circuit of Fig. 8*B* to that in Fig. 8*C*, by omitting those components which would have little effect on a slowly decaying response like the d.a.p.

Omitted components were the axoplasmic resistance, the nodal capacitance and the resistive and capacitative current pathways through the series of compact membranes of the myelin sheath. The axoplasmic resistance has a negligible effect on the d.a.p. because the action potential is conducted so rapidly that large lengths of axon are virtually isopotential during the d.a.p. Nodal capacitance is negligible compared to the internodal capacitance because the nodal membrane area is small compared to the internodal membrane area. Very little of the current from the internode will flow through the series of membranes of the myelin sheath, because their summed series resistance is very large and their effective series capacitance very small.

We then used our electrophysiological measurements to estimate the values of the circuit elements in the model of Fig. 8*C* for a typical large motor axon (outer fibre diameter 10–11 μm, estimated axon diameter 7 μm). Our calculations used an action potential amplitude of 75 mV and a d.a.p. amplitude of 10 mV. We assumed that the slow time constant of the axon membrane is 100 msec, the time constant of a typical d.a.p. in a hyperpolarized axon. If the d.a.p. is indeed a passive capacitative discharge, its time constant in a hyperpolarized axon, where the current–voltage relationship is linear over the voltage range traversed by the d.a.p. (Fig. 2*C*), should

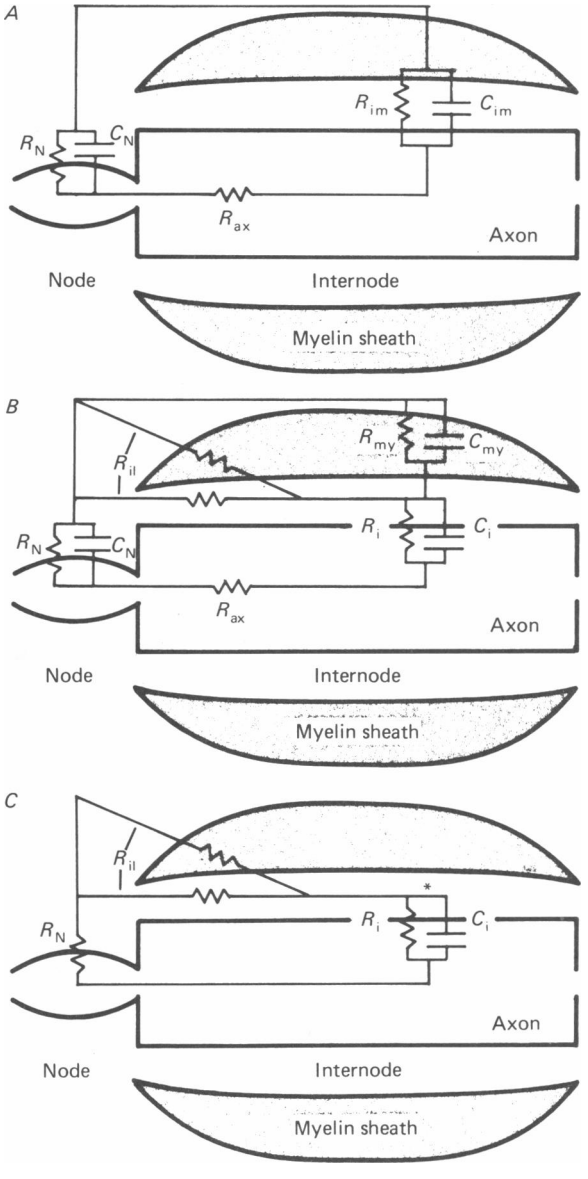

Fig. 8. Electrical models of the myelinated axon, superimposing electrical elements on a crude diagram of a node–internode segment. *A*, classical model, which lumps together the membranes of the internodal axon and the myelin sheath. *B*, suggested revised model, in which the internodal axon membrane discharges to ground via an internodal leakage resistance under or through the myelin sheath. *C*, revised model, simplified to include only those circuit elements which have an important effect on the slow depolarizing afterpotential (see text). R_N = resistance of nodal membrane, C_N = capacitance of nodal membrane, R_{ax} = resistance of axoplasm, R_{im} = lumped resistance of internodal axon and myelin sheath membranes in series, C_{im} = lumped capacitance of internodal axon and myelin sheath membranes in series, R_i = resistance of internodal axon membrane, C_i = capacitance of internodal axon membrane, R_{il} = internodal leakage resistance, R_{my} = resistance of myelin membranes in series, C_{my} = capacitance of myelin membranes in series. * denotes periaxonal space. Insertion of recorded d.a.p. parameters into the simplified model of *C* suggests that for a 1 cm length of a 7 μm diameter axon $c_i = 2{\cdot}2 \times 10^{-9}$ F/cm, $r_{il} = 9$ MΩcm, and the effective in parallel resistance of r_i and r_N is 45·5 MΩcm (see text and Appendix).

approximate the slow passive time constant of the axon membrane. As detailed in the Appendix and summarized in Table 1, these measurements and assumptions yield a membrane capacitance of $2{\cdot}2 \times 10^{-9}$ F/cm, an effective membrane resistance (r_E, equal to the nodal and internodal resistances added in parallel) of 45·5 MΩcm, and an internodal leakage resistance (r_{il}) of 9 MΩcm. This estimate of r_{il} is an underestimate when the recording system selectively attenuates the amplitude of the action potential (see Methods). For example, if the true action potential amplitude were 116 mV (Huxley & Stämpfli, 1951) instead of 75 mV, r_{il} would increase to 14 MΩcm.

TABLE 1. Quantitative description of model myelinated axon

Measured values	
Outer fibre diameter	10–11 μm
Action potential amplitude	75 mV
Peak amplitude of d.a.p. (mean)	10 mV
Time constant of decay of d.a.p.	100 msec
R_{in}, input resistance (mean)	88 MΩ
Assumed values	
d, axon diameter	7 μm[a]
ρ, axoplasm resistivity	110–114 Ωcm[b,h]
Distance between nodes	1 mm[c]
Specific membrane capacitance of axon	1 μF/cm²[d]
Number of layers of myelin	> 100[c]
Width of periaxonal space: internode	2–4 nm (large axons)[c]
	15–20 nm (small axons)
paranode	2–3 nm[c]
Length of myelin sheath attachment segment	2–4 μm[c]
Width of innermost layer of Schwann cell cytoplasm	10–25 nm[c]
Specific resistance of Schwann cell membrane	600 Ωcm²[d]
Number of Schmidt-Lanterman incisures per internode	20[e]
Cross-sectional area of Schmidt-Lanterman incisure	0·02–0·027 μm²[f]
Width of extracellular space within myelin	15–30 Å[g]
Calculated values	
c_E, c_i, capacitance of a 1 cm length of axonal membrane	$2{\cdot}2 \times 10^{-9}$ F/cm
r_E, effective resistance of a 1 cm length of axonal membrane (resistance of internodal and nodal membranes in parallel)	45·5 MΩcm
r_{il}, internodal leakage resistance of a 1 cm length of axon	9 MΩcm
R_N, input resistance of a single node (discrete model)	227 MΩ
R_a, axoplasmic resistance between two adjacent nodes	30 MΩ
R_{in}, calculated input resistance of myelinated axon	58–83 MΩ
$\boldsymbol{R}_E$, effective specific membrane resistance of nodal and internodal membranes added in parallel	10^5 Ωcm²
$\boldsymbol{R}_{il}$, specific resistance of internodal leak pathway	2×10^4 Ωcm²
$\lambda(\omega)$, space constant of axon for signals of the indicated frequencies	4·6 mm (0 Hz)
	2·5 mm (10–300 Hz)

[a] Landon & Hall (1976) give ratio of axon diameter to outer fibre diameter of 0·6–0·7.
[b] Tasaki (1955), toad peripheral nerve.
[c] Berthold (1978), cat peripheral nerve.
[d] Hodgkin (1964).
[e] Hiscoe (1947), rat peripheral nerve.
[f] Measured from Fig. 10 of Mugnaini *et al.* (1977), cat cochlear nerve.
[g] Schnapp & Mugnaini (1978), frog peripheral nerve.
[h] Schwarz, Neumcke & Stämpfli (1979), frog peripheral nerve.

These estimated resistance and capacitance values were assembled into an analogue circuit like that of Fig. 8*C*, and an action potential was simulated by injecting into this model axon a 3 msec current pulse that produced a depolarization of 75 mV. This simulated action potential has a voltage–time integral similar to that of our best recorded action potentials (200 mV msec). The model yields a depolarizing afterpotential closely resembling those recorded in real motor axons (compare Fig. 9*A* to Figs. 1*A* and *B* and 6).

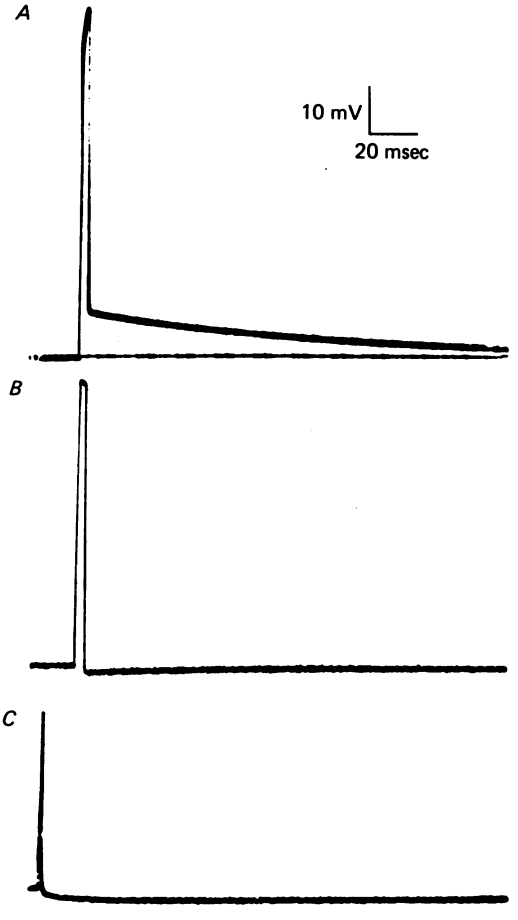

Fig. 9. *A* and *B*, intracellular (*A*) and periaxonal (*B*) voltage profiles produced by applying a simulated action potential to the analogue circuit of Fig. 8*C* (see text). *C*, action potential and hyperpolarizing afterpotential recorded from internodal region in the absence of a resting potential. The electrode tip was probably extra-axonal, in the myelin sheath or periaxonal space (see text). Same calibrations in *A*, *B* and *C*.

In some axons the d.a.p. is preceded by a brief plateau or hyperpolarizing 'dip' (e.g. Fig. 6*A*). We simulated this in the model axon by injecting a brief hyperpolarizing pulse immediately after the initial depolarizing pulse (not shown). As in real axons, the d.a.p. in the model axon rebuilds after an initial hyperpolarizing dip, since the brief hyperpolarization is not sufficient to dissipate all the charge on the internodal membrane capacitance.

Voltage sensitivity of the depolarizing afterpotential

The time integral ($\Delta V \times$ time) of a passive depolarizing afterpotential will be sensitive to the extent of charging of the internodal capacitance and to the input resistance of the axon during the d.a.p. These considerations help to explain the observed voltage sensitivity of the d.a.p. (Fig. 2): depolarization reduces the d.a.p. amplitude and the decay time by decreasing the amplitude of the action potential (thus decreasing the charging of the internodal capacitance) and, more importantly, by reducing the input resistance of the axon over the voltage range traversed during the d.a.p. (Fig. 2*C*).

Preliminary observations of the effect of tetraethylammonium ion (TEA), a K channel blocking agent, on the d.a.p. are also consistent with the passive discharge model. Even though it depolarizes the axon, TEA markedly increases the amplitude and time course of the d.a.p., probably because it prolongs the action potential and (via its K channel blocking properties) increases axonal input resistance (Scappaticci & Barrett, 1981).

Possible pathways for current flow from internode to bath

The morphology of myelinated axons suggests several possible routes for the postulated resistive current pathway between the internodal periaxonal space and the bath ground. We estimated the resistance of these pathways using the morphological measurements listed in Table 1, to determine whether any of these estimated pathway resistances fell close to the internodal leakage resistance of 9 MΩ cm calculated from electrophysiological measurements of the d.a.p. (see above and Appendix). Note that most of the morphological measurements come from mammalian (cat, rat, rabbit) peripheral nerve, the tissues used in the majority of the detailed morphological studies available to us. Most calculations used the formula $r = (\rho l)/A$, where r is the resistance of a particular pathway in a 1 cm length of axon, ρ is the resistivity of the medium (65 Ωcm for extracellular pathways, 114 Ωcm for intracellular pathways), and l and A are, respectively, the length and cross-sectional area of the pathway.

One possible leakage pathway is the periaxonal space, the extracellular space between the internodal axon membrane and the innermost layer of Schwann cell membrane (arrow 1, Fig. 10). This space is partially sealed off from the bath by the close (1–3 nm) apposition of the lateral loops of myelin and the axon in the paranodal region, but the space can be penetrated by extracellular markers such as horseradish peroxidase (myelinated fibres in newt, Krishnan & Singer, 1973; also reviewed by Schnapp & Mugnaini, 1978). According to Berthold (1978) the width of the periaxonal space in the internode of cat myelinated peripheral axons varies from 2–4 nm in large fibres to 15–20 nm in small fibres. Calculations using the morphological values listed in Table 1 suggest that the resistance of a current pathway through the periaxonal and paranodal extracellular space ranges from 42 to 400 MΩ cm, the exact value depending on the width of these spaces.

Another possible internodal leakage pathway is an intracellular pathway through the network of cytoplasmic belts in the Schwann cell (see Fig. 10, modified from Fig. 22 of Mugnaini *et al.* 1977). Current flowing from internode to bath through the cytoplasm of the Schwann cell would have to cross the Schwann cell membrane twice (upon entering and leaving the Schwann cell cytoplasm), but these membrane crossings would add less than 1 MΩ cm to the leakage resistance, assuming a value of 600 Ωcm^2 for the specific resistance of Schwann cell membranes. We calculated the resistance of two possible intracellular pathways, a pathway through the inner belt of Schwann cell cytoplasm (arrow 2, Fig. 10), and a spiral pathway through the clefts of Schmidt-Lanterman

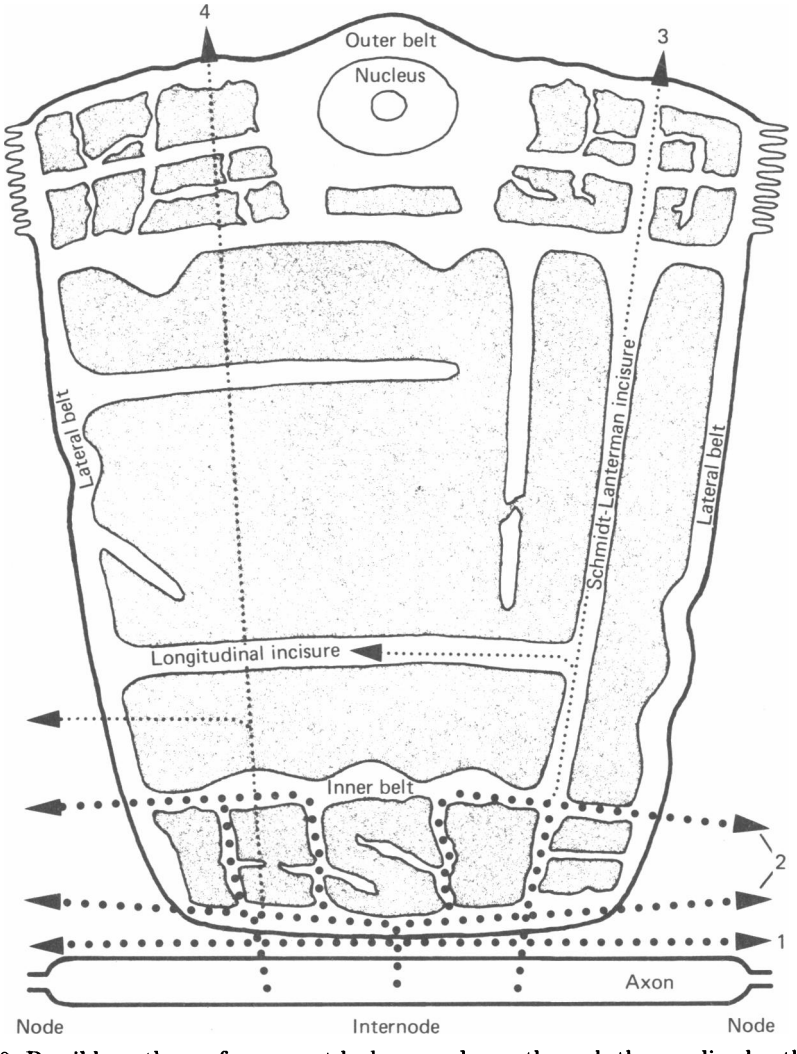

Fig. 10. Possible pathway for current leakage under or through the myelin sheath. This diagram of an 'unwrapped' myelin sheath in the peripheral nervous system is modified from Fig. 22 of Mugnaini *et al.* (1977). Dark areas denote regions of compact myelin; light areas cytoplasmic belts within the Schwann cell. The diagram is not to scale: the size of the cytoplasmic belts and of the innermost and outermost turns of the Schwann cell are greatly exaggerated. Dotted lines indicate possible pathways for the internodal leakage currents postulated in the text: (1) through the periaxonal space, (2) through the cytoplasm of the innermost turns of the Schwann cell, (3) spiral pathway through the clefts of Schmidt-Lanterman, and (4) spiral pathway through the thin water layer in compact myelin. Calculations based on available morphological measurements suggest that pathways 1 and 2 have the lowest resistance to current flow.

(arrow 3, Fig. 10). In cat peripheral nerve the width of the cytoplasm in the innermost turn of the Schwann cell is 10–25 nm (Berthold, 1978), which yields a resistance of 52–130 MΩ cm for this pathway in the axon of Table 1. A complete spiral pathway through the cytoplasm of the incisures of Schmidt-Lanterman (assuming twenty incisures per 1 mm node as found in rat peripheral axons by Hiscoe (1941) and a cross-sectional area of 0·02–0·03 μm^2, based on measurements from Fig. 10 of Mugnaini *et al.* 1977, for cat cochlear nerve) would have a resistance of 510–750 MΩ cm. However, most current entering the Schmidt-Lanterman incisures would leak out to the nodes via the longitudinal incisures, because the calculated length of a complete Schmidt-Lanterman incisure in the axon of Table 1 exceeds the length of a half-internode.

We also calculated the resistance of a spiral pathway through the extracellular water spaces of the compact myelin sheath, estimated to be 15–30 Å wide in frog peripheral myelinated axons (Schnapp & Mugnaini, 1978). There are morphological signs of tight junctions at both the internal and external openings (mesaxons) into the intramyelin extracellular space, but Coggeshall (1979) reports that in mammalian spinal roots the internal and external mesaxons are not completely sealed, suggesting that current can flow through this space. This spiral pathway would have a resistance of about 3–20 MΩ cm per turn of myelin around a 7 μm diameter axon, or about 300–2000 MΩcm for the 100+ myelin wraps around the axon of Table 1. Thus this particular current leakage pathway would be more important in smaller axons, which tend to have fewer myelin wraps.

While none of the estimated resistances of these possible internodal leakage pathways is as low as the value of 9 MΩ cm estimated from electrical measurements, these rough calculations do indicate that myelin morphology is compatible with the existence of substantial internodal leakage currents. The 'in-parallel' resistance of the two lowest resistance leakage pathways for the axon of Table 1, namely the periaxonal space and the innermost layers of Schwann cell cytoplasm, is about 25 MΩ cm, reasonably close to the electrical estimate. We expect some discrepancy between electrical and morphological estimates of the internodal leakage resistance, for several reasons. Our electrical estimate of leakage resistance is probably an underestimate, because of the frequency response of our recording system (see above and Methods), and because some current may leak through the myelin along the electrode track itself (although evidence cited above concerning the existance of substantial depolarizing afterpotentials in unimpaled internodes suggests that electrode-induced current leakage is not a major cause of the d.a.p.). Estimates of internodal leakage resistances calculated from available morphological data are probably over-estimates, because standard preparation of tissues for electron microscopy produces some shrinkage (Berthold, 1978). Paranodal morphology and the dimensions of the Schmidt-Lanterman incisures are known to be especially labile (Landon & Hall, 1976).

Consideration of axonal morphology predicts that the internodal leakage resistance will be lower, and consequently d.a.p. amplitude higher, in smaller axons. This is because smaller axons tend to have wider periaxonal spaces, fewer myelin wraps, and shorter internodal lengths than larger axons (Berthold, 1978). Also, smaller axons would be expected to have a higher average membrane resistance per unit length, and d.a.p. amplitude increases with the ratio of axonal membrane resistance to internodal leakage resistance. Our preliminary observations support this prediction: at a given membrane potential large sciatic axons (Fig. 1 *C*) tend to have smaller d.a.p. amplitudes than (presumably smaller) intramuscular axons, and motor axons near their terminals have larger d.a.p. amplitudes than motor axons prior to terminal branching. Also, factors that disrupt Schwann cell morphology (e.g. non-isotonic

solutions, demyelinating drugs such as lysophosphatidylcholine, and demyelinating diseases such as multiple sclerosis) should tend to decrease internodal leakage resistance and thus to increase d.a.p. amplitude.

Extra-axonal recordings from the internode

In a few cases (e.g. Fig. 9*C*) a micro-electrode inserted into an internodal region recorded 20–40 mV action potentials that were followed by a prolonged *hyper*polarization instead of the usual prolonged depolarization. There was little or no (< 10 mV) associated resting potential, suggesting that these unusual records originated outside the axon. Previous micro-electrode studies (Tasaki, 1952; Woodbury, 1952; Hardy, 1973) also reported recording action potentials of up to 30 mV amplitude in the absence of a normal resting potential. The polarity and substantial amplitude of the action potential suggest that in these cases the micro-electrode was in a space connected to the intra-axonal space by a relatively large capacitance, and isolated from the bath by a substantial resistance. We therefore suspect that these unusual records originated in the periaxonal space or somewhere within the myelin sheath. Injection of a simulated action potential into the axon model of Fig. 8*C* does produce in the periaxonal space (* in the Figure) a large action potential followed by a slowly decaying hyperpolarizing afterpotential (Fig. 9*B*). Thus, the passive membrane model of Fig. 8*C* can account (at least qualitatively) for both the depolarizing afterpotential recorded intra-axonally and the hyperpolarizing afterpotential recorded in or near the periaxonal space.

The different time course of the predicted (Fig. 9*B*) and observed (Fig. 9*C*) hyperpolarizing afterpotentials may reflect non-uniform charging of the internodal membrane capacitance during the action potential. If, as we suspect, the major pathways for internodal leakage current are through the periaxonal space and the innermost layer of Schwann cell cytoplasm, the distributed nature of this resistance will make the axonal membranes nearest the node (which have a lower leakage resistance to ground) charge more quickly than membranes near the middle of the internode. This non-uniform charging will give rise to redistribution currents along the periaxonal space, especially during the early portion of the d.a.p.

Axonal space constant as a function of signal frequency

The revised electrical model of the myelinated axon that we propose (Fig. 8*B*) predicts a different frequency dependence for the axonal space constant, λ, than the classical model (Fig. 8*A*). The classical model predicts that λ should remain approximately constant for signal frequencies between 0 and at least 300 Hz, and then decrease with further increases in signal frequency. Our revised model predicts that λ should begin to decrease at frequencies as low as 1 Hz, and after decreasing about 50% should reach a plateau in the frequency range 10–300 Hz, decreasing again at higher signal frequencies. The plateau in the intermediate frequency range occurs because at these frequencies most of the membrane current will pass through the large internodal axonal membrane capacitance, bypassing the high internodal axonal membrane resistance. This capacitative current will be limited only by the smaller internodal series leak resistance. Thus in this frequency range, which includes much of the frequency power spectrum of the action potential, the axonal space constant

(λ) will be determined primarily by the resistance of the internodal leakage pathway (r_{il}), the axoplasm resistivity (ρ), and the inner diameter of the axon (d):

$$\lambda_{10\text{–}300\ \mathrm{Hz}} = \tfrac{1}{2}d\sqrt{(\pi r_{il}/\rho)}.$$

The value of r_{il} used in our model predicts a value of 2·5 mm for λ in this intermediate frequency range. Since nodes in these peripheral axons are about 1 mm apart, this λ value is compatible with saltatory conduction. If r_{il} decreases (for example, during a demyelinating disease), the space constant also decreases, jeopardizing action potential conduction.

The space constant predicted for very low frequency signals (0 to 1 Hz) is longer, about 4·1–4·6 mm, since at low frequencies the internodal axonal membrane resistance is no longer bypassed by the capacitative current route. Thus slow potential changes like the d.a.p. would be propagated passively for a considerable distance along a myelinated axon. We have occasionally even recorded slow, d.a.p.-like potentials propagating in the absence of the fast action potential, but have not investigated this phenomenon in detail.

Functional importance of axonal depolarizing afterpotential

The depolarizing afterpotential in the peripheral axons studied here appears to be primarily a passive depolarization. This passive afterdepolarization would be expected to increase axonal excitability, and indeed Raymond (1979) demonstrated that frog sciatic axons have a prolonged superexcitable period, whose time course is very similar to that of the d.a.p. we record. Our preliminary observations in lizard axons also indicate that axonal excitability is increased during the d.a.p. This superexcitable period could thus be important in conducting high-frequency repetitive activity through regions with a low safety factor for conduction, such as axonal branch points, short demyelinated segments, or unmyelinated nerve terminals (see Raymond, 1979). Action potentials arising during a superexcitable period will also have a faster conduction velocity, so that prior activity in an axon will alter both the probability and the velocity of subsequent impulse transmission in that axon (Swadlow & Waxman, 1976).

Our calculations and preliminary observations (Fig. 1) suggest that the amplitude of the d.a.p. is larger in smaller axons, and increases as the axon approaches its terminal. If this prediction proves true, the d.a.p. that propagates electrotonically into the unmyelinated motor nerve terminal may be quite large, and may contribute to the repetitive discharge of motor nerve terminals observed under certain experimental conditions (see review of Miyamoto, 1978). The postulated prolonged terminal depolarization may also contribute to the prolonged elevation of miniature end-plate potential frequency that follows the end-plate potential (delayed release, Rahamimoff & Yaari, 1973). However, it seems unlikely that the d.a.p. is a rate-limiting factor in the facilitation of evoked transmitter release observed during repetitive nerve stimulation (Mallart & Martin, 1967; Magleby, 1973). The d.a.p. and facilitation have similar time courses at room temperature, but the time course of facilitation slows markedly as the temperature is lowered from 20 to 10 °C (Balnave & Gage, 1974), while the time course of the d.a.p. changes little over this temperature range (Fig. 6).

Depolarizing afterpotentials in other axons

Preliminary intracellular recordings from rat ventral root axons *in situ* also exhibit a depolarizing afterpotential (Fig. 11). This d.a.p. decays much more rapidly than the d.a.p.s seen in lizard and frog axons. This shorter duration is consistent with reports that the 'supernormal' (superexcitable) period and the whole-nerve negative afterpotential (depolarizing afterpotential) in large peripheral axons (A fibres) are shorter in mammals than in frogs (Gasser, 1937). We do not yet know whether the d.a.p. in rat peripheral axons is mediated by internodal leakage currents. However, the quantitative analysis presented above suggests that all myelinated axons have some internodal leakage currents.

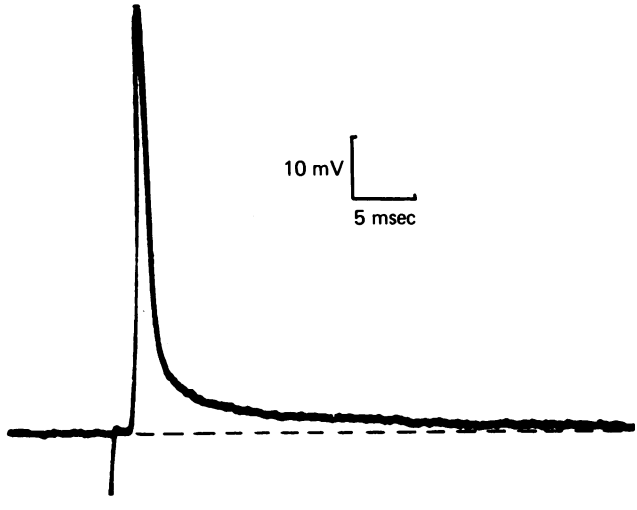

Fig. 11. Action potential and depolarizing afterpotential recorded intracellularly from a rat ventral root axon *in situ* (terminals intact). The d.a.p. is briefer than that in frog and lizard axons.

Depolarizing afterpotentials and post-stimulus superexcitable periods are by no means limited to myelinated axons. The whole nerve recordings of Grundfest & Gasser (1938) showed that unmyelinated C fibres of the mammalian hypogastric nerve have a post-stimulus superexcitable period with the same time course as the negative afterpotential. More recently, Gardner-Medwin (1972) demonstrated a large superexcitable period in unmyelinated cerebellar parallel fibres, and Waxman & Swadlow (1976) report that both myelinated and unmyelinated visual callosal fibres in rabbit have superexcitable periods. Depolarizing afterpotentials have been recorded in terminal and preterminal regions of single, unmyelinated crayfish motor axons (Dudel, 1973; Fuchs & Getting, 1980), and these terminals have a post-stimulus superexcitable period (Zucker, 1974). The reported durations of the superexcitable periods in these various axons range from 5–250 msec. The mechanisms of the superexcitable periods in these other axons, and of the depolarizing afterpotentials that have been shown or inferred to underly them, are as yet unknown. Many have been attributed to extracellular K accumulation, because in some axons super-

excitability and/or the magnitude of the (extracellularly recorded) depolarizing afterpotential are reduced when bath [K] is elevated (Zucker, 1974). However, our results indicate that it is important to distinguish the K sensitivity of the d.a.p. from its voltage sensitivity. In lizard axons the effect of bath [K] on d.a.p. amplitude appears to be indirect, mediated by K effects on membrane potential, because d.a.p. sensitivity to bath [K] disappears when membrane potential is held constant (Fig. 5). Also, the d.a.p. following single action potentials in frog axons is not prolonged by cooling (Fig. 6) or ouabain, treatments expected to slow the rate of active K uptake.

It is conceivable that the d.a.p. postulated in unmyelinated axons might, like the d.a.p. in some myelinated axons, represent a passive capacitative discharge. Unmyelinated axons would show a long passive d.a.p. if the axonal membrane has a high specific membrane resistance, and hence a long passive time constant, and if activation of axonal K channels requires relatively large depolarizations, so that most of the K channels activated during the action potential close before the axon has completely repolarized. If this model is accurate, then the time course of the d.a.p. in unmyelinated axons would, as in some myelinated axons, reflect a passive time constant of the axonal membrane. Axonal time constants of 100 msec or more have been reported; for example, Hudspeth, Poo & Stuart (1977) describe barnacle photoreceptors whose average passive membrane time constant exceeds 300 msec.

APPENDIX

Estimation of axonal electrophysiological characteristics

Effective axonal membrane resistance, r_E

The effective membrane resistance in the axon model of Fig. 8*C* can be estimated from the time constant of the d.a.p. in hyperpolarized axons, $\tau_{d.a.p.}$, which should approximate the slow time constant of the axon membrane (see text). Thus $\tau_{d.a.p}$ should be approximately equal to the product of the effective membrane capacitance, c_E, times the effective resistance of the circuit, r_E:

$$\tau_{d.a.p.} = c_E r_E. \tag{1}$$

Only the nodal and internodal axon membrane resistances need be considered in estimating r_E, because the existence of a significant long-time-constant current pathway in myelinated axons in itself argues that the internodal leakage resistance, r_{il}, is small compared to the effective membrane resistance of the axon. Thus, r_E is approximately equal to the resistances of the nodal (r_N) and internodal (r_i) axonal membranes added in parallel:

$$r_E \cong \frac{r_i \cdot r_N}{r_i + r_N}.$$

Assuming that the axonal membrane (which consists mostly of internodal membrane) has a specific membrane capacitance of 1 μF/cm^2 (see Table 1), the capacitance of a 1 cm length of membrane in our larger motor axons (estimated 7 μm diameter) is $2{\cdot}2 \times 10^{-9}$ F/cm. Using a reasonable $\tau_{d.a.p}$ value of 100 msec, eqn (1) yields a value of 45·5 MΩcm for the effective resistance of a 1 cm length of this axon (effective specific resistance, $\boldsymbol{R}_E$, of 10^5 Ωcm^2).

As an internal check on the consistency of the model of Fig. 8*C*, we calculated the

range of axonal input resistance (R_{in}) values compatible with the model and compared it to the range of R_{in} values (67–118 MΩ) measured in our larger (7 μm diameter) motor axons.

The upper limit of the input resistance values compatible with the model was calculated using a 'discrete' version of the model, which assumes that the input resistance in resting axons is determined mainly by the nodal resistance, i.e. that for a 1 cm length of axon the internodal membrane resistance r_i is much larger than the nodal membrane resistance r_N. Using our estimated value for axonal diameter ($d = 7$ μm) and assumed values for internodal distance (1 mm) and axoplasmic resistivity ($\rho = 114$ Ωcm) (see Table 1), this discrete version of the model predicts that the axoplasmic resistance between two nodes (R_a) is 30 MΩ, and that the input resistance of a single node (R_N) is 227 MΩ. This value for R_N is higher than the value of 40–124 MΩ given for frog nodes by Tasaki (1955) and Conti *et al.* (1976) (see Results section on axonal input resistance). The calculated input resistance (R_{in}) at an internode in the centre of such a multinodal network, given by:

$$R_{in} = \tfrac{1}{4}\sqrt{(R_a{}^2 + 4R_a R_N)}$$

is 83 MΩ.

A lower limit for R_{in} was calculated assuming that R_{in} is dominated by r_i. This version of the model essentially assumes that the axon is a uniform core conductor, because the internodal membrane area is much larger than the nodal membrane area. R_{in}, given by the core conductor equation:

$$R_{in} = \frac{1}{\pi}\sqrt{\frac{R_E \rho}{d^3}}$$

equals 58 MΩ.

Models assuming that both nodal and internodal membranes make significant contributions to the resting input resistance (e.g. Tasaki, 1955) yield R_{in} values intermediate between the two extremes (58 and 83 MΩ) calculated above.

Thus, regardless of the exact distribution of the resting membrane resistance between the internodal and nodal axonal membranes, the model of Fig. 8*C* yields input resistance values (58–83 MΩ) close to the range of values measured experimentally in 7 μm diameter motor axons (67–118 MΩ). Our measured R_{in} values are probably higher than those that would be measured in the infinite 7 μm diameter axon assumed in the calculations, because distal to our recording sites the motor axon branches and narrows to closed-end terminals. Predicted R_{in} values would increase if axoplasmic resistivity (ρ) were 160- Ωcm (Chiu, Ritchie, Rogart & Stagg, 1979) instead of the assumed 114 Ωcm.

Internodal leakage resistance, r_{il}

The leakage resistance from the internodal periaxonal space to ground, r_{il}, was estimated from the ratio of the peak amplitudes of the action potential and d.a.p., which was 75 mV/10 mV (or 7·5 : 1) in our healthiest motor axons. We injected a 3 msec, 75 mV pulse simulating the action potential into the axon model of Fig. 8*C*, and determined the value of r_{il} required to give a 10 mV simulated d.a.p. The use of a single lumped circuit (Fig. 8*C*) to estimate r_{il} is justified because the rapid conduction of the action potential (estimated at 20 mm/msec for a myelinated axon

with an outer diameter of 10 μm, Tasaki, 1953) makes long segments of the axon (more than 20 mm, much greater than the space constant) virtually isopotential during the slow d.a.p. The simulated action potential, though unaccompanied by the normal nodal conductance changes, should charge the internodal capacitance to the same extent as a real action potential. The value of r_{il} so determined was 9·1 MΩcm for the discrete version of the axon model (see above), 8·6 MΩcm for the uniform core conductor version. The simulated d.a.p. had the same exponential decay (τ = 100 msec) regardless of how the total resting membrane resistance was partitioned between nodal and internodal axonal membranes. The specific internodal leakage resistance ($\boldsymbol{R}_{il}$) was 2×10^4 Ωcm^2.

We thank Dr K. Scappaticci for permission to cite work in progress, R. Andreu for help in the initial phases of these experiments, and A. Cosio, G. Cabrera and M. Wolf for help in preparing the manuscript. The work was supported by grants NS 12404 and NS 12207 from the National Institutes of Health.

REFERENCES

ÅRHEM, P. (1980). Effects of some heavy metal ions on the ionic currents of myelinated fibres from *Xenopus laevis*. *J. Physiol.* **306**, 219–231.

BALNAVE, R. J. & GAGE, P. W. (1974). On facilitation of transmitter release at the toad neuromuscular junction. *J. Physiol.* **239**, 657–675.

BARRETT, E. F. & BARRETT, J. N. (1976). Separation of two voltage-sensitive potassium currents, and demonstration of a tetrodotoxin-resistant calcium current in frog motoneurones. *J. Physiol.* **255**, 737–774.

BERTHOLD, C.-H. (1978). Morphology of normal peripheral axons. In *Physiology and Pathobiology of Axons*, ed. WAXMAN, S. G., pp. 3–63. New York: Raven Press.

CHIU, S. Y., RITCHIE, J. M., ROGART, R. B. & STAGG, D. (1979). A quantitative description of membrane currents in rabbit myelinated nerve. *J. Physiol.* **292**, 149–166.

COGGESHALL, R. E. (1979). The myelin sheath in mammalian spinal roots. *Anat. Rec.* **193**, 508.

CONTI, F., HILLE, B., NEUMCKE, B., NONNER, W. & STÄMPFLI, R. (1976). Measurement of the conductance of the sodium channel from current fluctuations at the node of Ranvier. *J. Physiol.* **262**, 699–727.

DUDEL, J. (1973). Recording of action potentials and polarization of a single crayfish motor axon through a sucrose-gap capillary suction electrode. *Pflügers Arch.* **338**, 187–199.

FUCHS, P. A. & GETTING, P. A. (1980). Ionic basis of presynaptic inhibitory potentials at crayfish claw opener. *J. Neurophysiol.* **43**, 1547–1557.

GARDNER-MEDWIN, A. R. (1972). An extreme supernormal period in cerebellar parallel fibres. *J. Physiol.* **222**, 357–371.

GASSER, H. S. (1937). Sequence of potential changes, and the excitability cycle. In *Electrical Signs of Nervous Activity*, by ERLANGER, J. & GASSER, H. S. pp. 130–205 in 2nd edition (1968). Philadelphia: Univ. of Pennsylvania Press.

GRUNDFEST, H. & GASSER, H. S. (1938). Properties of mammalian nerve fibres of slowest conduction. *Am. J. Physiol.* **123**, 307–318.

HARDY, W. L. (1973). Propagation speed in myelinated nerve I. Experimental dependence on external Na^+ and on temperature. *Biophys. J.* **13**, 1054–1070.

HILLE, B., WOODHULL, A. M. & SHAPIRO, B. J. (1975). Negative surface charge near sodium channels of nerve: divalent ions, monovalent ions and pH. *Phil. Trans. R. Soc.* B **270**, 301–318.

HISCOE, H. B. (1947). Distribution of nodes and incisures in normal and regenerated nerve fibres. *Anat. Rec.* **99**, 447–475.

HODGKIN, A. L. (1964). *The Conduction of the Nervous Impulse*. Springfield, Illinois: Charles C. Thomas.

HUDSPETH, A. J., POO, M. M. & STUART, A. E. (1977). Passive signal propagation and membrane properties in median photoreceptors of the giant barnacle. *J. Physiol.* **272**, 25–43.

HUXLEY, A. F. & STÄMPFLI, R. (1951). Direct determination of membrane resting potential and action potential in single myelinated nerve fibres. *J. Physiol.* **112**, 476–495.

KRISHNAN, N. & SINGER, M. (1973). Penetration of peroxidase into peripheral nerve fibers. *Am. J. Anat.* **136**, 1–14.

LANDON, D. N. & HALL, S. (1976). The myelinated nerve fiber. In *The Peripheral Nerve*, ed. LANDON, D. N., pp. 1–105. London: Chapman & Hall.

MAGLEBY, K. (1973). The effect of repetitive stimulation on facilitation of transmitter release at the frog neuromuscular junction. *J. Physiol.* **234**, 327–352.

MALLART, A. & MARTIN, A. R. (1967). An analysis of facilitation of transmitter release at the neuromuscular junction of the frog. *J. Physiol.* **193**, 679–694.

MIYAMOTO, M. D. (1978). The actions of cholinergic drugs on motor nerve terminals. *Pharmac. Rev.* **29**, 221–247.

MUGNAINI, E., OSEN, K. K., SCHNAPP, B. & FREIDRICH, V. L., JR. (1977). Distribution of Schwann cell cytoplasm and plasmalemmal vesicles (caveolae) in peripheral myelin sheaths. An electron microscopic study with thin sections and freeze-fracturing. *J. Neurocytol.* **6**, 647–668.

OGDEN, T. E., CITRON, M. C. & PIERANTONI, R. (1978). The jet stream microbeveler: an inexpensive way to bevel ultrafine glass micropipettes. *Science, N.Y.* **201**, 469–470.

RAHAMIMOFF, R. & YAARI, Y. (1973). Delayed release of transmitter at the frog neuromuscular junction. *J. Physiol.* **228**, 241–257.

RAYMOND, S. A. (1979). Effects of nerve impulses on threshold of frog sciatic nerve fibres. *J. Physiol.* **290**, 273–303.

SCAPPATICCI, K. A. & BARRETT, E. F. (1981). TEA enhances the depolarizing afterpotential in single myelinated axons. *Neurosci. Abstr.* **7**, (in the Press).

SCHNAPP, B. & MUGNAINI, E. (1978). Membrane architecture of myelinated fibers as seen by freeze-fracture. In *Physiology and Pathobiology of Axons*, ed. WAXMAN, S. G., pp. 83–123. New York: Raven Press.

SCHWARZ, W., NEUMCKE, B. & STÄMPFLI, R. (1979). Longitudinal resistance of axoplasm in myelinated nerve fibers of the frog. *Pflügers Arch.* **379**, R41.

STÄMPFLI, R. (1952). Bau und Funktion isolierter markhaltiger Nervenfasern. *Ergebn. Physiol.* **47**, 70–165.

SWADLOW, H. A. & WAXMAN, S. G. (1976). Variations in conduction velocity and excitability following single and multiple impulses of visual callosal axons in the rabbit. *Expl Neurol.* **53**, 128–150.

TASAKI, I. (1952). Properties of myelinated fibers in frog sciatic nerve and in spinal cord as examined with micro-electrodes. *Jap. J. Physiol.* **3**, 73–94.

TASAKI, I. (1953). *Nervous Transmission.* Springfield, Illinois: Charles C. Thomas.

TASAKI, I. (1955). New measurements of the capacity and the resistance of the myelin sheath and the nodal membrane of the isolated frog nerve fiber. *Am. J. Physiol.* **181**, 639–650.

TASAKI, I. & FRANK, K. (1955). Measurement of the action potential of myelinated nerve fiber. *Am. J. Physiol.* **182**, 572–578.

WAXMAN, S. G. & SWADLOW, H. A. (1976). Morphology and physiology of visual callosal axons: evidence for a supernormal period in central myelinated axons. *Brain Res.* **113**, 179–187.

WOODBURY, J. W. (1952). Direct membrane resting and action potentials from single myelinated nerve fibers. *J. cell. comp. Physiol.* **39**, 323–339.

ZUCKER, R. S. (1974). Excitability changes in crayfish motor neurone terminals. *J. Physiol.* **241**, 111–126.